Cavity Enhanced absorption spectroscopy with an Optical Comb: Detection of atmospheric radicals in the near UV

ARTICLE · APRIL 2009

READS
27

3 AUTHORS, INCLUDING:

Guillaume Méjean
University Joseph Fourier - Grenoble 1
60 PUBLICATIONS **2,255** CITATIONS

SEE PROFILE

Environmental Science & Technology

Article

pubs.acs.org/est

Frequency Comb Based Spectrometer for *in Situ* and Real Time Measurements of IO, BrO, NO_2, and H_2CO at pptv and ppqv Levels

Roberto Grilli,[†] Guillaume Méjean,[†] Samir Kassi,[†] Irène Ventrillard,[†] Chadi Abd-Alrahman,[†] and Daniele Romanini*,[†]

[†]University Grenoble 1/CNRS, LIPhy UMR 5588, Grenoble, F-38041, France

Supporting Information

ABSTRACT: We report an instrument designed for trace gas measurement of highly reactive halogenated radicals, such as bromine oxide and iodine oxide, as well as for nitrogen dioxide and formaldehyde. This compact and robust spectrometer relies on an alternated injection of a frequency-doubled femtosecond radiation at 338 and 436 nm into two parallel high-finesse cavities, for measuring BrO, H_2CO, IO, and NO_2, respectively. The transmission of the broadband radiation through the cavity is analyzed with a high resolution, compact spectrograph consisting of an echelle grating and a high sensitivity CCD camera. The transportable instrument fits on a breadboard 120 × 60 cm size and is suitable for *in situ* and real time measurements of these species. A field campaign at the Marine Boundary Layer in Roscoff (in the northwest of France, 48.7°N, 4.0°W) during June 2011 illustrates the outstanding performance of the instrument, which reaches a bandwidth normalized minimum absorption coefficient of 1.3×10^{-11} cm^{-1} $Hz^{-1/2}$ per spectral element, and provides detection levels as low as 20 parts per quadrillion of IO in 5 min of acquisition.

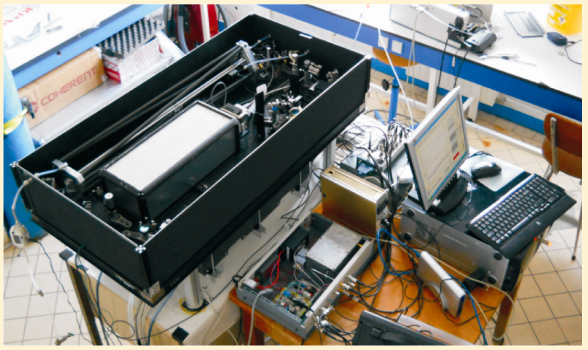

1. INTRODUCTION

The chemistry and photochemistry of iodine and bromine compounds in the atmosphere, with a particular interest to the highly reactive forms such as the halogen oxides, have progressively captured the attention of the atmospheric community aiming at a better understanding of their oxidizing capacity of Earth's troposphere.[1] During springtime in the Polar Regions, reactive bromine, chlorine, and iodine compounds are responsible for the rapid ozone depletion in the Marine Boundary Layer (MBL).[2] Halogen oxides are also known to be involved in the oxidation of gaseous elemental Hg[3] and dimethyl sulfide (DMS),[4,5] both employed as tracers to reconstruct climatic conditions that prevailed during the Earth's history and to get an insight about the oxidative processes taking place in the atmosphere as a response to global warming.

Measurements of halogen oxides molecules have been performed in the last years using different techniques, each with its advantages and drawbacks. Laser Induced Fluorescence (LIF) presented by Whalley et al.[6] to measure IO shows a detection limit of 0.3 pptv (part per trillion by volume, $1{:}10^{12}$) within 300 s of acquisition. Chemical ionization mass spectrometry may provide detection limits down to 2.6 pptv for IO radical within 4 s of integration time.[7,8] However, both techniques suffer of not being absolute analytical methods and require regular calibrations using standard samples. Up to now, absorption spectroscopy methods employed for field measurements mainly lead to nonspatially resolved techniques such as long-path differential optical absorption spectroscopy (LP-DOAS)[1] or multiaxis differential optical absorption spectroscopy (Max-DOAS)[9,10] using incoherent radiation. On one hand, these techniques offer a large versatility thanks to the spectral coverage of the light source, allowing the monitoring of multiple species. On the other hand, no local information on concentrations is provided because the measurements are integrated over atmospheric volumes which are several km thick (either vertically or horizontally). In addition, the performances of the open path techniques strongly depend on climatic conditions. The atmospheric box-model calculations performed by Burkholder et al.[11] on the iodine chemistry at the MBL highlight the issue that long-path techniques do not sufficiently account for the presence of inhomogeneous sources of iodine, leading to a mismatch between experimental measurements and calculations. Wada et al. demonstrated an open path cavity ring-down spectrometer for IO measurements injecting a pulsed dye laser into a high-finesse cavity and providing a detection limit of 10 pptv [12] which is, however, not sufficient in most atmospheric situations. Finally, the cavity enhanced absorption spectroscopy (CEAS)

Special Issue: Marine Boundary Layer: Ocean Atmospheric Interactions

Received: May 9, 2012
Revised: July 18, 2012
Accepted: August 13, 2012

dx.doi.org/10.1021/es301785h | *Environ. Sci. Technol.* XXXX, XXX, XXX–XXX

technique has been already exploited by Kasyutich et al. in an off-axis configuration using a violet laser diode,[13] while Vaughan et al. employed an incoherent broad-band cavity enhanced configuration (IBBCEAS)[14] for the detection of IO, NO_2 and IO, OIO and I_2, respectively. Both techniques show a good performance for discharge-flow kinetic studies in the laboratory, while detection limits of 140 and 210 pptv for the IO radical were achieved, which are not sufficient for measurements in the field.

Here, an instrument based on mode-locked cavity enhanced absorption spectroscopy (ML-CEAS) is presented. This instrument is robust and transportable and offers real time, *in situ*, local measurements of BrO, H_2CO, IO, and NO_2. Thanks to its high sensitivity, field measurements in very remote environments are therefore feasible. The spectrometer addresses the near UV-visible spectral region where a large number of strong and characteristic electronic transitions of relevant atmospheric molecules are present. [15] The use of a broadband femtosecond laser, continuously tunable from 675 to 1080 nm, allows for accessing the whole spectral region from the green to the near UV (337 to 540 nm) by frequency doubling, providing high versatility as a trace gas analyzer for several relevant atmospheric species.

2. EXPERIMENTAL SETUP

The instrument consists of a compact femtosecond laser oscillator (100−250 fs, 80 MHz, Chameleon, Coherent Inc.) which provides 700 mW of average power within 2 nm of bandwidth centered at 677 nm and 2.5 W within 5 nm of bandwidth at 871 nm. The laser head is fixed under a 120 × 60 × 6 cm^3 aluminum honeycomb breadboard, while the rest of the optical setup is placed above. The laser radiation is frequency doubled with a 0.2 mm thick, type-I, BBO (β-barium borate) crystal (Fujian CASTECH Crystals, Inc.). The thickness and the focusing lens (f = 30 mm) are chosen to get a good compromise between maximizing the second harmonic generation while keeping a small walk-off and preventing astigmatism of the harmonic output beam due to chromatic dispersion. The BBO crystal is mounted on a motorized rotation stage (AG-PR100, Newport) that allows computer controlled phase-matching optimization, which is important when the wavelength is switched from 677 to 871 nm. The conversion efficiency for the frequency doubling is 4% W^{-1}, and in the wavelength domain the width of the second harmonic radiation is reduced by a factor of $2\sqrt{2}$ with respect to the one of the fundamental radiation. Three dichroic steering mirrors, used as band-pass filters, clean the beam from the fundamental beam before injecting the optical cavity. An acousto-optic modulator (AOM) with 80% efficiency on the first order diffracted beam acts as a fast optical switch and a programmable attenuator. On one hand, it allows for regularly performing ring-down measurements in the absence of absorbents for determining the cavity finesse, as explained in the data analysis section. On the other hand, the AOM is also used to attenuate the 436 nm radiation by a factor of ∼5; although a high cavity finesse and a loose locking scheme are employed, the CCD camera electronic wells become saturated even at the shortest integration time (12 ms) (see Figure 1).

The laser beam is spatially mode matched to the TEM_{00} mode of the cavity with a single lens (f = 750 mm) placed after the doubling crystal. A special design of the high finesse cell provides the highest stability to fulfill field campaign constraints. The 94-cm long double high-finesse linear cavity

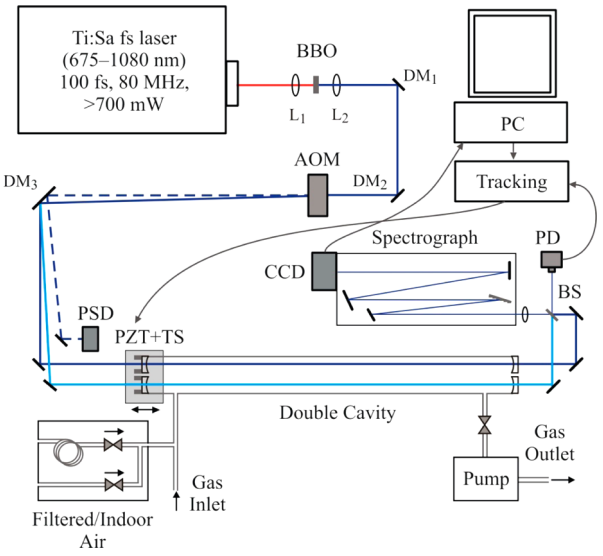

Figure 1. Schematic diagram of the experimental setup. The fundamental radiation from the femtosecond Ti:Sa laser is frequency doubled using a β-barium borate crystal (BBO) and injected into a parallel 94-cm long double cavity. The mode matching to the resonator is achieved by the lens L_2, and the cavity length is modulated around a comb resonance using a tracking circuit controlling a piezo electric transducer (PZT). The transmitted beam is divided by a 50:50 beam splitter (BS) toward a photodiode (PD) and a compact high resolution spectrograph. The mounts of the dichroic stirring mirror (DM_3), grating, BBO crystal, and the cavity translation stage (TS) are motorized and controlled by software. Automatic software driven control routines allow for maintaining system alignment and high signal during long-term measurements. AOM: acousto-optic modulator, PSD: photosensitive detector, CCD: charge-coupled device.

is architected around six carbon bars mounted in a telescope-like arrangement (inspired to the Serrurier truss used in Dobsonian telescopes [16]). A motorized translation stage (T-LS28, Zaber) is incorporated in the cavity to adjust its free spectral range (FSR) to be twice the laser repetition rate. On one side of the cavity, mirrors are mounted on two independent piezo-electric tube transducers (PZT, type PT130.20, PI France S.A.S.) to modulate the cavity length across the resonance condition and finely adjust the average FSR. To obtain this condition a tracking circuit, similar to the one proposed by Romanini et al.,[17] is employed to compensate for laser jitter and mechanical instabilities (vibrations and drifts) of the system by applying a correction signal to the PZT together with a fast sinusoidal modulation (20 kHz and 5 kHz at 338 and 436 nm, respectively). This type of tracking scheme is advantageous when a free running frequency comb oscillator has to be injected into an optical resonator. Contrary to other more sophisticated tight locking schemes, a modulation with tracking ensures the injection of the whole spectral comb even when the selected comb resonance is not perfect. This scheme is therefore insensitive to cavity dispersion that would induce a nonuniform cavity mode spacing which ultimately frustrates perfect comb matching, and it does not require a control of the central frequency of the laser comb as well as its repetition rate. This scheme is such that the comb modes all go through resonance with the same speed but with some harmless temporal dispersion.[18,19] This allows for recovering the full laser spectrum transmitted without distortion by the cavity and integrating it on the CCD detector during several successive passages through resonance. The two sets of cavity mirrors

dx.doi.org/10.1021/es301785h | Environ. Sci. Technol. XXXX, XXX, XXX−XXX

(Layertec) are selected for their maximal reflectivity of 99.948% and 99.990% at 338 and 436 nm, respectively. They are prealigned before being glued on aluminum holders which can be removed for mirrors cleaning propose and replaced without affecting the optical alignment. After the cavity, a beam splitter is equally dividing the beam onto a photodiode and through a homemade compact spectrograph providing ∼5 pm (0.45 cm^{-1}) spectral resolution. The spectrograph is composed of a high order diffraction grating (Thorlabs, GE2550-0863, blaze angle = 63°, 79 grooves per mm, 25 × 50 mm^2 size) and a high-sensitivity blue enhanced (back-thinned) TE-cooled CCD camera (Hamamatsu, C10151, 2048 × 250 $pixels^2$). A full description of the spectrograph is provided by Grilli et al.[21] The spectrograph was realized for the detection of the halogen oxides radicals, probing strong electronic transitions. The broadening of these absorption bands is limited by the lifetime broadening of the transitions, since the excited states are predissociatives. For those reasons, a resolution of 5 pm is already enough to reach the best enhancement in terms of contrast of the spectra of IO and BrO. However, a resolution of 2 pm (corresponding to a chromatic resolving power of 2 × 10^5) could be achieved by reducing the focal of the entrance lens from 40 to 10 mm, which it would increase the sensitivity for the detection of NO_2 and H_2CO.

The gas line is entirely composed of PFA (Perfluoroalkoxy), which has been found to be the best tubing material to efficiently transport highly reactive radical species, such as BrO and IO,[21] as well as the reactive hydrogen fluoride, HF.[22] At the cavity output, a diaphragm pump and a manual proportional valve are employed to provide a gas flow of 800 sccm (standard cubic centimeters). The cavity inlet can sample three different lines through a cross connection. The first line is the outdoor air that is collected with a 6 mm diameter PFA tube. The second line is linked to a filtered air generator, composed of a second diaphragm pump, a particle filter, and a scrubber that are employed to provide a flow rate greater than 800 sccm which dynamically replaces the input flow. This filtered air flow, free of NO_2, IO, and BrO, is switched on/off by a software controlled electrovalve and allows for acquiring reference spectra and ring-down events essential for absorption scale absolute calibration. However, formaldehyde is not completely removed by this filtering system, and an additional filter, such as the commercial Hopcalite, is required to remove volatile organic compounds from the air sample; in alternative a zero air cylinder can be employed to acquire reference spectra, which is, however, less practical for field campaign propose. A second electrovalve allows for partially collecting no filter indoor air which is naturally enriched in NO_2 and H_2CO: the recognition of their spectra by the fitting routine allows for adjusting the fit parameters (in particular the spectral centering, as explained in the Supporting Information).

The whole spectrometer is confined in an aluminum box covered by a thermal insulating material and temperature stabilized at 26 °C with a peltier air-air exchanger (Supercool, AA-040-12-22) module coupled to a PID temperature controller (Supercool, TC-PR-59). The data analysis is performed in real time by homemade software and discussed in Section 3. The tuning of the laser frequency is also controlled by software; however, the switch between the detection of BrO - CH_2O and IO - NO_2 still requires the operator support, and it can be performed in ∼10 min since the optical components are all prealigned, except for the BBO crystal, the DM3, and the grating which are mounted on motorized stages, and therefore controlled by software. The total weight of the system is 250 kg, and the power consumption is 3 kW.

Data Analysis. This section describes the data analysis performed by the Labview software to retrieve the concentrations of the target molecules. Thanks to the transient coupling of the laser to the cavity, the ML-CEAS scheme can be considered equivalent to broadband cavity enhanced absorption spectroscopy (BB-CEAS). [19] In BB-CEAS the frequency dependent absorption coefficient can be expressed as a function of the transmission spectrum, $T(\nu) = I(\nu)/I_0(\nu)$, and the ring-down time of the empty cavity, τ_0[23]

$$\alpha(\nu) = \left(\frac{I_0(\nu)}{I(\nu)} - 1\right)\frac{1}{\tau_0 c} \quad (1)$$

where c is the speed of light. The ring-down time is measured by performing cavity ring-down spectroscopy (CRDS)[24] when zero air is continuously flowing into the cavity at 800 sccm at atmospheric pressure. In our calculations τ_0 corresponds to an average photon lifetime of the entire broad-band radiation circulating inside the cavity, and the product $\tau_0 c$ is the inverse of the effective path length obtained in the absence of absorbers. We may assume that this parameter, proportional to the finesse, is almost constant over the injected laser spectrum which is spectrally narrow relative to the mirror reflection band. The transmission spectrum is calculated as the ratio between the laser spectrum transmitted through the cavity in the presence, $I(\nu)$, and in the absence, $I_0(\nu)$, of the absorbers, after subtracting from both the CCD camera background (taken with the laser beam interrupted by the AOM). Spectral data, $\alpha(\nu)$, are analyzed in real time by a standard linear multicomponent fit routine,[25] where spectra of known concentrations of analytes, α_i, are used as references for the fit, and the coefficient, c_i (c_{BrO}, c_{IO}, etc.), are giving the sample concentrations

$$\alpha(\nu) = \sum_i \alpha_i(\nu)\cdot c_i + p(\nu)\ (i = BrO, \quad H_2CO \text{ or } IO, \quad NO_2) \quad (2)$$

where $p(\nu)$ is a polynomial function, which accounts for a spectral shift of the laser between the acquisition of $I(\nu)$ and $I_0(\nu)$ together with the presence of broad and unstructured absorption features may present. The reference spectra are experimental data acquired by our ML-CEAS instrument, which are inherently taking into account the instrumental function and the wavelength calibration of our spectrometer. The concentrations of the reference spectra were calculated by using the wavelength dependent absorption cross sections found in the literature for BrO,[26,27] H_2CO,[28] IO,[29,30] and NO_2.[31] The uncertainty of the measurement for the radical species is limited by the uncertainty of the literature absorption cross sections (evaluated to be about 10% for the halogen oxides), while the precision on the measured ring-down times is better than 1%.

The detection limits expressed as bandwidth normalized minimum absorption coefficient per spectral element, $\alpha_{min}(BW)$, are calculated by the following equation

$$\alpha_{min}(BW) = \frac{\Delta I_{min}}{I_0}\frac{1}{\tau_0 c}\cdot\left(\frac{t}{M}\right)^{1/2} \quad (3)$$

where I_0 is the cavity output intensity, ΔI_{min} represents the minimum detectable change of the output intensity, t is the

dx.doi.org/10.1021/es301785h | Environ. Sci. Technol. XXXX, XXX, XXX−XXX

integration time, and M is the number of independent spectral elements (corresponding to 1000 and 1500 for the detection at 338 and 436 nm, respectively). By fitting the ratio between two consecutive acquisitions at the CCD camera with a polynomial of the same order of $p(\nu)$, the ΔI_{min} for a single acquisition can therefore be calculated (which corresponds to the rms of the fit). Furthermore, monitoring ΔI_{min} during the acquisition allows for rejecting in real time data which are more affected by mechanical instabilities. This will cause some dead time during acquisition, which will not exceed the 10% of the total acquisition time. For our instrument, $\alpha_{min}(BW)$ are 1.6×10^{-10} and 1.3×10^{-11} cm^{-1} $Hz^{-1/2}$ per spectral element, at 338 and 436 nm, respectively. From the experimental spectra, detection limits expressed in terms of minimum detectable mixing ratio at atmospheric pressure are calculated: 1 pptv and 100 ppt are attended within 1 min of integration for BrO and H_2CO, respectively, and 20 ppqv and 5 pptv are obtained within 5 min of integration for IO and NO_2, respectively. Here, the intrinsic structure of the molecular spectra plays an important role, which leads to a lower detection limit for IO with respect to BrO, together with the greater cavity finesse and a better laser stability, as discussed in the Results section. As already proved by Grilli et al., [19] the instrument provides experimental spectra which are close to the shot noise limit.

3. RESULTS AND DISCUSSION

Examples of typical low-concentration spectra obtained around 338.5 and 436 nm are displayed in Figures 2 and 3, respectively.

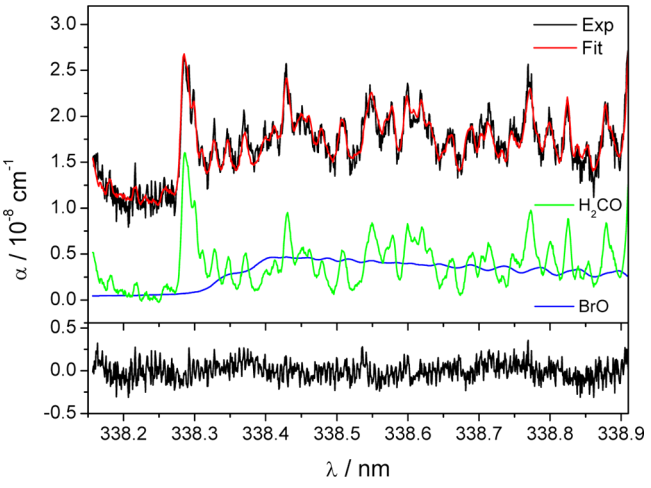

Figure 2. A typical low concentration spectrum of BrO and H_2CO obtained around 338.5 nm with 26 s of acquisition time. The blue and the green traces are the reference spectra of BrO (corresponding to 8.9 pptv) and H_2CO (corresponding to 5.6 ppbv), respectively. Experimental data (black) and fit (red) were offset by 10^{-8} cm^{-1} for better display. Fit residuals are reported at the bottom and correspond to a rms value of 1.0×10^{-9} cm^{-1}.

For the detection of BrO and H_2CO, a cavity with a finesse of 6,000 was employed, corresponding to a mirror reflectivity R = 99.948% and leading to an effective path length of 1.8 km. The normalized noise equivalent absorption achieved was $\alpha_{min} = 1.6 \times 10^{-10}$ cm^{-1} $Hz^{-1/2}$ per spectral element, corresponding to detection limits of 7 pptv and 730 pptv for BrO and H_2CO, respectively, for 1 s of acquisition. Better results were achieved for the detection around 436 nm, where higher reflectivity mirrors (R = 99.990%, finesse of 32,000) are commercially

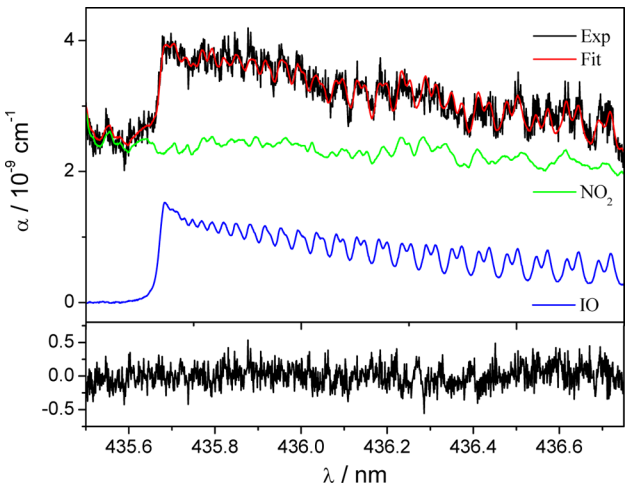

Figure 3. A typical spectrum of low concentration IO and NO_2 recorded around 436 nm. The experimental data and the fit are reported in black and red, respectively, and the reference spectrum of IO (corresponding to 1 pptv) and NO_2 (corresponding to 150 pptv) are shown in blue and green, respectively. With an acquisition time of 12 s a detection limit of 60 ppqv and 11 pptv of IO and NO_2 were achieved. The residuals of the fit are reported in the bottom window, corresponding to a rms of 1.5×10^{-10} cm^{-1}.

available, together with a more stable operation of the Ti:Sapphire laser at this wavelength (fundamental wavelength = 872 nm). With the 10 km equivalent optical path length a normalized noise equivalent absorption of 1.3×10^{-11} cm^{-1} $Hz^{-1/2}$ per spectral element was achieved, and detection limits of 200 ppqv and 40 pptv of IO and NO_2, respectively, were obtained when the signal was integrated for 1 s. In the experimental and the fitted trend of Figure 2 an offset of 10^{-8} cm^{-1} was deliberately added for display purposes, while in Figure 3 the offset is naturally provided by the spectrum of NO_2 which is a quasi-continuum absorption over this wavelength region.

To study the long-term stability of the system, Allan variance tests[32] were performed at the two wavelengths. Due to high reactivity and chemical properties of halogen oxide molecules it is difficult if not impossible to obtain a stable source of these analytes, thus real outdoor air containing NO_2 and H_2CO but no IO and BrO was continuously flowed to the cavity during the stability tests. The instrument analyses spectra averaged over 10 acquisitions, while the reference spectra (in the presence of zero air) was recorded at the beginning of the measurement averaging 10k spectra. The time for an individual acquisition as needed to attain close to saturation of the CCD was 26 and 12 ms for the BrO and IO, respectively. Fluctuation due to changes in the composition of the outdoor air are visible on the nitrogen oxide and formaldehyde trace, while due to the absence of the halogen oxide radicals source nearby our laboratory, a concentration fluctuating around zero is observed for IO and BrO. Allan standard deviation for the BrO is reported in the log−log plot of Figure 4, where white noise is dominating for about 20 s, and the trend reaches a minimum value of 1 pptv after ∼1 min. At longer integration time, a leveling or tendency to a slight increasing of the Allan deviation appears, mainly due to a poor laser stability when running close to the limit of its tuning range (677 nm). The same data analysis was performed for zero levels of IO in the presence (top right) and the absence (top left) of NO_2 and reported in

dx.doi.org/10.1021/es301785h | Environ. Sci. Technol. XXXX, XXX, XXX−XXX

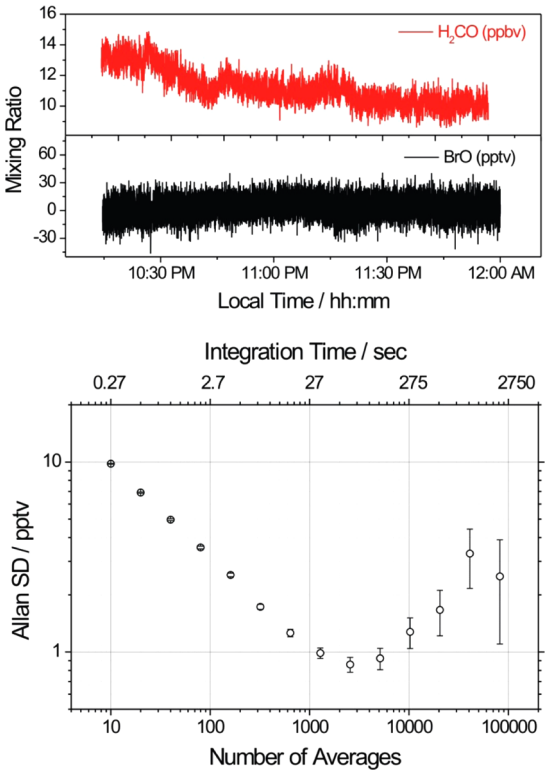

Figure 4. The top window reports long-term measurements of H_2CO and BrO for outdoor air sampled outside our laboratory (in the absence of BrO). Each spectrum was acquired after averaging 10 consecutive acquisition (260 ms) before being fitted. The bottom plot shows the Allan standard deviation for the derived BrO concentration around zero. The experimental trend follows the white noise for ~20 s, reaching a minimum value of ~1 pptv after 1 min integration.

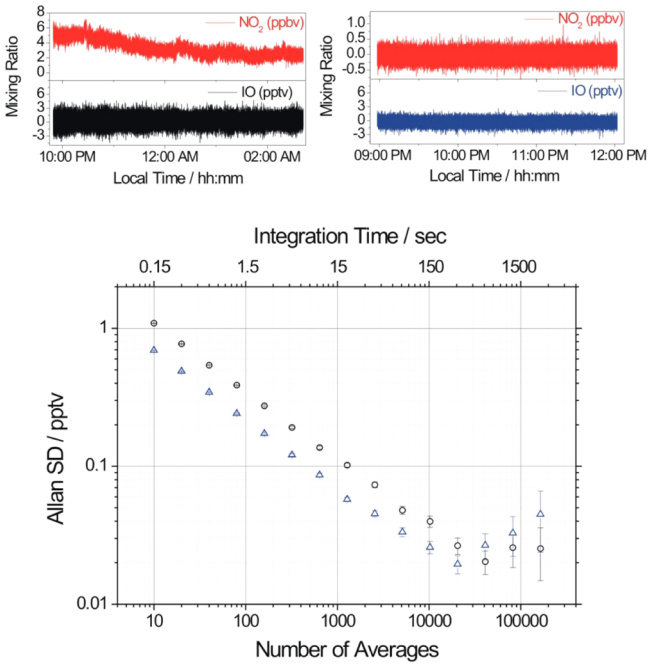

Figure 5. The top plots reports the long-term measurements of the air outside our laboratory (left) and filtered air (right) where zero levels of IO are attended. Each acquired spectrum is averaged 10 times before being fitted. The Allan variance plot for the IO in the presence of NO_2 (black circles) and with filtered air (blue triangles) is shown in the log−log plot at the bottom. A lower noise level is observed in the absence of NO_2, confirming the presence of a residual structure of NO_2 after the fit. The system follows the white noise for more than 2 min, reaching a minimum of 20 ppqv after 5 min integration time.

f5 the bottom plot of Figure 5. The presence of high concentrations of NO_2 (black dots) gives an Allan standard deviation trend higher than what it is observed in the case of zero level of NO_2 (blue triangles). This can be explained by the presence of a residual structure of NO_2 after the fit. In this presence of zero or low level of NO_2, the standard deviation of the residue is in agreement with the spectrum shown in Figure 3, and the detection limit reaches a minimum value of 20 ppqv (parts per quadrillion by volume, $1{:}10^{15}$) after 5 min of acquisition. It should be noticed that the performance of the instrument in the laboratory and in the field are identical, leading to the same stability results as well as the same detection limits at both wavelengths. Moreover, the residual structure on NO_2 after the fit, which becomes significant for relatively high concentrations, could be removed by taking the reference spectrum for the fit in the same condition of the measurement (i.e., spectrometer temperature, laser alignment, etc). It should be noticed that a concentration of NO_2 3 orders of magnitude above its detection limit only increases the detection limit of the IO radical by a factor of 2.

A field campaign was carried out at the CNRS "Station Biologique de Roscoff" (SBR) in the northwest coast of France (48.7°N 4.0°W), during June 2011. The presence of halogen oxides radicals in the semipolluted area of Roscoff is due to the active microalgae metabolism together with the large tidal amplitudes, which provides an increase of the seaweeds exposure during the low tide. For the displacement of the instrument, the laser head was detached from the breadboard and transported in a separate case. The rest of the spectrometer (optics, cavity, and spectrograph) was left on the breadboard, while the electronics and the gas manifold were also disassembled and transported separately. Pictures of the apparatus are available in the Supporting Information. Reassembling and optimizing the whole setup took about one day for two expert operators.

During the field campaign, long-term measurements of BrO, H_2CO, IO, and NO_2 were performed on outdoor air. A continuous flow of 800 sccm was provided by the membrane pump placed after the cavity, and the experimental spectra were fitted in real time by the program containing the multi-component fit routine. An example of a long-term measurement of BrO and H_2CO is reported in Figure 6. An increasing f6 of the concentration of BrO up to 4 (±1) pptv was observed on June 21st in correspondence to a low tide with a coefficient of 62 at 17h00. Our observation is in agreement with previews measurement performed by Mahajan et al.[33] in the same site using the LP-DOAS technique. Figure 7 shows long-term f7 measurements of IO and NO_2 where a better vertical and temporal resolution is achieved thanks to the higher performances of the instrument at this wavelength region. An anticorrelation between the concentration of IO and NO_2 is observed as expected in a semipolluted environment due to their reaction to form $IONO_2$. An increase in concentration of NO_2 at ppbv (parts per billion by volume, $1{:}10^9$) levels, in fact, leads to a depletion of IO radical in the atmosphere. $XONO_2$ is known to be a temporary reservoir of halogen atoms in an NO_x-rich environment.[34] In the period between 10h00 and 11h00 in the morning a drop in concentration of IO was

dx.doi.org/10.1021/es301785h | Environ. Sci. Technol. XXXX, XXX, XXX−XXX

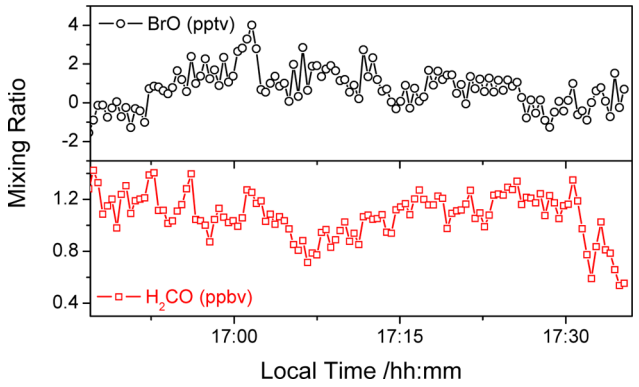

Figure 6. MBL long-term measurements of BrO and H_2CO at the SBR of Roscoff (France) (48.7°N, 40°W). The measurements were performed on June 21st 2011 when a low tide (tidal coefficient = 62) occurred around 17 h, corresponding with a maximum in concentration of BrO. The detection limits are 1 and 100 pptv for BrO and H_2CO, respectively.

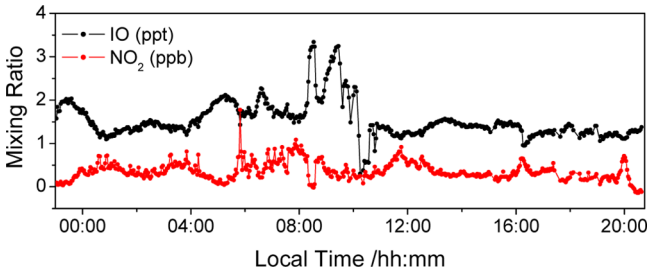

Figure 7. MBL long-term measurements of IO and NO_2 performed at the SBR of Roscoff (France) (48.7°N, 40°W). The measurements were performed on June 18th 2011. Concentrations of IO of few pptv were observed during the day, and a strong anticorrelation with the concentration of NO_2 was observed, as expected in a semipolluted environment. No particular correlation with the tide level was noticed. The detection limits are 20 ppqv and 5 pptv for IO and NO_2, respectively.

observed, while no changes in NO_2 concentration were observed. No particular investigations have been done at this propose, but a change in the meteorological conditions (particularly wind speed and direction) and therefore of the air mass analyzed could explain this behavior.

A transportable instrument based on mode-locked cavity-enhanced absorption spectroscopy to measure pptv and subpptv levels of atmospherically important halogen oxide radicals is reported here. Thanks to the double-cavity setup, alternative measurements of BrO and IO at 338 and 436 nm, respectively, were possible. The bandwidth normalized minimum absorption coefficients are 1.6×10^{-10} and 1.3×10^{-11} cm^{-1} $Hz^{-1/2}$ per spectral element, at 338 and 436 nm, respectively.

Due to the broad-band character of the instrument, H_2CO and NO_2 could also be measured by the instrument together with the halogen oxides which were the principal target species of this development. This compact and robust instrument is finally suitable for *in situ* measurements of local concentrations of BrO, H_2CO, IO, and NO_2, providing detection limits of 1 pptv (1 min), 100 ppt (1 min), 20 ppqv (5 min), and 5 pptv (5 min), respectively. The sensitivity of the instrument can be improved by increasing the cavity finesse, even if the mirrors which have been selected here are the ones currently available in the market with the highest reflectivities at these wavelengths. Increasing the number of photons would also lead to an increasing of the sensitivity, but it requires a CCD camera or a photodiode array with deeper quantum wells. However, the laser power should be kept below the limit where bleaching of the halogen oxides radicals occurs. A further improvement in the stability of the femtosecond laser at 677 nm will also enhance the detection of BrO and H_2CO, by integrating the signal for a longer time.

The large tunability of the system would allow for extending the number of molecules detectable, with the possibility to include other environmental important species such as OClO, HONO, OIO, etc. Moreover, by frequency tripling the fundamental radiation probing the strong rotational transitions of the OH radical at 308 nm is promising. Because of the high stability of the femtosecond oscillator at the corresponding fundamental wavelength, a minimum measurable extinction coefficient of 5×10^{-5} $Hz^{-1/2}$ (comparable to the performance obtained at 436 nm for 5 min average) can be achieved, leading to sensitivity down to the 10^5 radicals/cm^{-3} with a 1 km path length allowed by mirror coatings available at 308 nm, which would be enough to detect the OH radical in the atmosphere.

■ ASSOCIATED CONTENT

Supporting Information

Detailed description of the automatisms of the setup employed to reoptimize the signal quality and to make the system working as a standalone instrument during long-term measurement. Two pictures of the instrument. This material is available free of charge via the Internet at http://pubs.acs.org.

■ AUTHOR INFORMATION

Corresponding Author

*Phone: +33 (0) 4.76.51.47.67. Fax: +33 (0) 4.76.63.54.95. E-mail: daniel.romanini@ujf-grenoble.fr.

Notes

The authors declare no competing financial interest.

■ ACKNOWLEDGMENTS

We are grateful to Jean-Luc Martin from LIPhy for his skilled technical help on several details of the setup, to Philippe Potin and Chaterine Leblanc, SBR, Roscoff for the help during the field campaign, and to Robert Georges, IPR, Rennes, for providing local support. We acknowledge financial support from ANR (Contract ANR-09-BLAN-0016), from the "Reseau Technologique Femtoseconde" of CNRS and from our laboratory LIPhy.

■ REFERENCES

(1) Saiz-Lopez, A.; Mahajan, A. S.; Salmon, R. A.; Bauguitte, S. J.-B.; Jones, A. E.; Roscoe, H. K.; Plane, J. M. C. Boundary layer halogens in coastal Antarctica. *Science* **2007**, *317*, 348−351, DOI: 10.1126/science.1141408.

(2) Barrie, L. A.; Bottenheim, J. W.; Schnell, R. C.; Crutzen, P. J.; Rasmussen, R. A. Ozone destruction and photochemical reactions at polar sunrise in the lower Arctic atmosphere. *Nature* **1988**, *334*, 138−141, DOI: 10.1038/334138a0.

(3) Lindberg, S. E.; Brooks, S.; Lin, C.-J.; Scott, K. J.; Landis, M. S.; Stevens, R. K.; Goodsite, M.; Richter, A. Dynamic oxidation of gaseous mercury in the Arctic troposphere at polar sunrise. *Environ. Sci. Technol.* **2002**, *36*, 1245−1256, DOI: 10.1021/es0111941.

(4) Preunkert, S.; Jourdain, B.; Legrand, M.; Udisti, R.; Becagli, S.; Cerri, O. Seasonality of sulfur species (dimethyl sulfide, sulfate, and methanesulfonate) in Antarctica: inland versus coastal regions. *J. Geophys. Res.* **2008**, *113*, D15302 DOI: 10.1029/2008JD009937.

(5) Read, K. A.; Lewis, A. C.; Bauguitte, S.; Rankin, A. M.; Salmon, R. A.; Wolff, E. W.; Saiz-Lopez, A.; Bloss, W. J.; Heard, D. E.; Lee, J. D.; Plane, J. M. C. DMS and MSA measurements in the Antarctic boundary layer: impact of BrO on MSA production. *Atmos. Chem. Phys. Discuss.* **2008**, *8*, 2657−2694.

(6) Whalley, L. K.; Furneaux, K. L.; Gravestock, T.; Atkinson, H. M.; Bale, C. S. E.; Ingham, T.; Bloss, W. J.; Heard, D. E. Detection of iodine monoxide radicals in the marine boundary layer using laser induced fluorescence spectroscopy. *J. Atmos. Chem.* **2007**, *58*, 19−39, DOI: 10.1007/s10874-007-9075-9.

(7) Munson, M. S. B.; Field, F. H. Chemical ionization mass spectrometry. I. general introduction. *J. Am. Chem. Soc.* **1966**, *88*, 2621−2630, DOI: 10.1021/ja00964a001.

(8) Liao, J.; Sihler, H.; Huey, L. G.; Neuman, J. A.; Tanner, D. J.; Friess, U.; Platt, U.; Flocke, F. M.; Orlando, J. J.; Shepson, P. B.; Beine, H. J.; Weinheimer, A. J.; Sjostedt, S. J.; Nowak, J. B.; Knapp, D. J.; Staebler, R. M.; Zheng, W.; Sander, R.; Hall, S. R.; Ullmann, K. A comparison of Arctic BrO measurements by chemical ionization mass spectrometry and long path-differential optical absorption spectroscopy. *J. Geophys. Res.* **2011**, *116*, D00R02 DOI: 10.1029/2010JD014788.

(9) Hönninger, G.; Platt, U. Observations of BrO and its vertical distribution during surface ozone depletion at Alert. *Atmos. Environ.* **2002**, *36*, 2481−2489, DOI: 10.1016/S1352-2310(02)00104-8.

(10) Coburn, S.; Dix; Sinreich, R.; Volkamer, R. The CU ground MAX-DOAS instrument: characterization of RMS noise limitations and first measurements near Pensacola, FL of BrO, IO, and CHOCHO. *Atmos. Meas. Tech.* **2011**, *4*, 2421−2439, DOI: 10.5194/amt-4-2421-2011.

(11) Burkholder, J. B.; Curtius, J.; Ravishankara, A. R.; Lovejoy, E. R. Laboratory studies of the homogeneous nucleation of iodine oxides. *Atmos. Chem. Phys.* **2004**, *4*, 19−34, DOI: 1680-7324/acp/2004-4-19.

(12) Wada, R.; Beames, J. M.; Orr-Ewing, A. J. Measurement of IO radical concentrations in the marine boundary layer using a cavity ring-down spectrometer. *J. Atmos. Chem.* **2007**, *58*, 69−87, DOI: DOI 10.1007/s10874-007-9080-z.

(13) Kasyutich, V. L.; Bale, C. S. E.; Canosa-mas, C. E.; Pfrang, C.; Vaughan, S.; Wayne, R. P. Cavity-enhanced absorption: detection of nitrogen dioxide and iodine monoxide using a violet laser diode. *Appl. Phys. B: Lasers Opt.* **2003**, *76*, 691−697, DOI: 10.1007/s00340-003-1153-3.

(14) Vaughan, S.; Gherman, T.; Ruth, A. A.; Orphal, J. Incoherent broad-band cavity-enhanced absorption spectroscopy of the marine boundary layer species I_2, IO and OIO. *Phys. Chem. Chem. Phys.* **2008**, *10*, 4471−4477, DOI: 10.1039/B802618A.

(15) Orphal, J.; Chance, K. Ultraviolet and visible absorption cross-sections for HITRAN. *J. Quant. Spectrosc. Radiat. Transfer* **2003**, *82*, 491−504, DOI: 10.1016/S0022-4073(03)00173-0.

(16) Kriege, D.; Berry, R. *The Dobsonian Telescope: A Practical Manual for Building Large Aperture Telescopes*; Willmann-Bell: 1997; ISBN 0-943396-55-7.

(17) Romanini, D.; Kachanov, A. A.; Sadeghi, N.; Stoeckel, E. CW cavity ring down spectroscopy. *Chem. Phys. Lett.* **1997**, *264*, 316−322, DOI: 10.1016/S0009-2614(96)01351-6.

(18) Gherman, T.; Romanini, D. Modelocked cavity-enhanced absorption spectroscopy. *Opt. Express* **2002**, *10*, 1033.

(19) Grilli, R.; Méjean, G.; Abd Alrahman, C.; Ventrillard, I.; Kassi, S.; Romanini, D. Cavity-enhanced multiplexed comb spectroscopy down to the photon shot noise. *Phys. Rev. A* **2012**, *85*, 051804(R) DOI: 10.1103/PhysRevA.85.051804.

(20) Thorpe, M. J.; Ye, J. Cavity-enhanced direct frequency comb spectroscopy. *Appl. Phys. B: Lasers Opt.* **2008**, *91*, 397−414, DOI: 10.1007/s00340-008-3019-1.

(21) Grilli, R.; Méjean, G.; Kassi, S.; Ventrillard, I.; Abd-Alrahman, C.; Fasci, E.; Romanini, D. Trace measurement of BrO at the ppt level by a transportable mode-locked frequency-doubled cavity-enhanced spectrometer. *Appl. Phys. B: Lasers Opt.* **2012**, *107*, 205−212, DOI: 10.1007/s00340-011-4812-9.

(22) Aghnatios, C.; Pailloux, A.; Weulersse, J.-M.; Romanini, D. Private communication.

(23) Triki, M.; Cermak, P.; Méjean, G.; Romanini, D. Cavity-enhanced absorption spectroscopy with a red LED source for NO_x trace analysis. *Appl. Phys. B: Lasers Opt.* **2008**, *91*, 195−201, DOI: 10.1007/s00340-008-2958-x.

(24) O'Keefe, A.; Deacon, D. A. G. Cavity ring-down optical spectrometer for absorption measurements using pulsed laser sources. *Rev. Sci. Instrum.* **1988**, *59*, 2544.

(25) Press, W. H.; Teukolsky, S.; Vetterling, W.; Flannery, B. *Numerical Recipes in C. The Art of Scientific Computing*, 2nd ed.; Cambridge University Press: 1992.

(26) Wilmouth, D. M.; Hanisco, T. F.; Donahue, N. M.; Anderson, J. G. Fourier transform ultraviolet spectroscopy of the A $2\Pi_{3/2}$← X $2\Pi_{3/2}$ transition of BrO. *J. Phys. Chem. A* **1999**, *103*, 8935−8945, DOI: 10.1021/jp991651o.

(27) Fleischmann, O. C.; Hartmann, M.; Burrows, J. P.; Orphal, J. New ultraviolet absorption cross-sections of BrO at atmospheric temperatures measured by time-windowing Fourier transform spectroscopy. *J. Photochem. Photobiol., A* **2004**, *168*, 117−132, DOI: 10.1016/j.jphotochem.2004.03.026.

(28) Smith, C. A.; Pope, F. D.; Cronin, B.; Parkes, C. B.; Orr-Ewing, A. J. Absorption cross sections of formaldehyde at wavelengths from 300 to 340 nm at 294 and 245 K. *J. Phys. Chem. A* **2006**, *110* (41), 11645−11653, DOI: 10.1021/jp063713y.

(29) Newman, S. M.; Howie, W. H.; Lane, I. C.; Upson, M. R.; Orr-Ewing, A. J. Predissociation of the A $2\Pi_{3/2}$ state of IO studied by cavity ring-down spectroscopy. *J. Chem. Soc., Faraday Trans.* **1998**, *94*, 2681−2688, DOI: DOI: 10.1039/A805103H.

(30) Nakano, Y.; Enami, S.; Nakamichi, S.; Aloisio, S.; Hashimoto, S.; Kawasaki, M. Temperature and pressure dependence study of the reaction of IO radicals with dimethyl sulfide by cavity ring-down laser spectroscopy. *J. Phys. Chem. A* **2003**, *107*, 6381−6387, DOI: 10.1021/jp0345147.

(31) Nizkorodov, S. A.; Sanderr, S. P.; Brown, L. R. Temperature and pressure dependence of high-resolution air-broadened absorption cross sections of NO2 (415−525 nm). *J. Phys. Chem. A* **2004**, *108*, 4864−4872, DOI: DOI: 10.1021/jp049461n.

(32) Werle, P. Accuracy and precision of laser spectrometers for trace gas sensing in the presence of optical fringes and atmospheric turbulence. *Appl. Phys. B: Lasers Opt.* **2011**, *102*, 313−329, DOI: 10.1007/s00340-010-4165-9.

(33) Mahajan, A. S.; Oetjen, H.; Lee, J. D.; Saiz-Lopez, A.; McFiggans, G. B.; Plane, J. M. C. High bromine oxide concentrations in the semi-polluted boundary layer. *Atmos. Environ.* **2009**, *43*, 3811−3818, DOI: 10.1016/j.atmosenv.2009.05.033.

(34) Vogt, R.; Sander, R.; Von Glasow, R.; Crutzen, P. Iodine chemistry and its role in halogen activation and ozone loss in the marine boundary layer: a model study. *J. Atmos. Chem.* **1999**, *32*, 375−395, DOI: 10.1023/A:1006179901037.